Semiconductor Physics, Quantum Electronics & Optoelectronics, 2023. V. 26, No 3. P. 260-269.

Semiconductor physics

Relationship between oxidation, stresses, morphology, local resistivity, and optical properties of TiO_2, Gd_2O_3, Er_2O_3, SiO_2 thin films on SiC

O.B. Okhrimenko[1*], Yu.Yu. Bacherikov[1], P.M. Lytvyn[1], O.S. Lytvyn[1,2], V.Yu. Goroneskul[1], R.V. Konakova[1]

[1]*V. Lashkaryov Institute of Semiconductor Physics, NAS of Ukraine, 41, prospect Nauky, 03680 Kyiv, Ukraine*
[2]*Borys Grinchenko Kyiv University, 18/2, Bulvarno-Kudriavska str., Kyiv, Ukraine*
[*]*Corresponding author e-mail: olga@isp.kiev.ua*

Abstract. The relationship between internal mechanical stresses, surface morphology, nanoscale electrical properties, and optical characteristics in TiO_2, Gd_2O_3, Er_2O_3, and SiO_2 thin films on SiC substrates was investigated. The oxide films were synthesized using the rapid thermal annealing and analyzed through scanning spreading resistance microscopy, photoluminescence, and absorption spectroscopy. Tensile stresses were found in the films, they are attributed to thermal and lattice mismatch, oxidation, and grain boundaries. These stresses influence on surface morphology, resistivity variations, and photoluminescence intensity. Surface roughness and grain structure were found to correlate with variations in resistivity, which were attributed to conductive pathways along grain boundaries and possible metallic phases. Photoluminescence intensity was also observed to correlate with estimated lattice mismatch strain. Gd_2O_3/SiC exhibited the fewest defects, while Er_2O_3 and TiO_2 showed more, with Er_2O_3 being the most mismatched and roughest. The results indicate that internal strains in oxide thin films on SiC substrates can influence on surface morphology, leading to formation of defects and spatial inhomogeneity. These fluctuations in local conductivity and luminescence center density have significant implications for dielectric and optical applications. The study provides insights for future processing refinements to mitigate internal strains and enhance the performance of oxide thin films in semiconductor and optical technologies.

Keywords: TiO_2, Gd_2O_3, Er_2O_3, stresses**,** oxide/semiconductor structures, absorption, photoluminescence, scanning spreading resistance microscopy.

https://doi.org/10.15407/spqeo26.03.260
PACS 68.37.-d, 68.55.J-, 68.60.Bs, 73.61.-r, 78.20.-e, 78.55.Hx

Manuscript received 27.06.23; revised version received 19.07.23; accepted for publication 13.09.23; published online 20.09.23.

1. Introduction

Oxide/semiconductor (OS) structures are one of the most demanded functional elements of semiconductor electronics. OS structures are used to create photoresistors, dynamic memory elements, as a gate in field-effect transistors, *etc*. The quality of interface in these structures largely defines the performance of metal-dielectric-semiconductor (MIS) structures [1–15]. Also, oxide films are widely used for optical coatings, protective coatings, in photocatalysis, gas sensors, biocompatible coatings, *etc.* [16–19]. OS structures are commonly applied in electronic technology, where silicon or silicon carbide are used as semiconductors, and silicon oxide usually acts as a traditional oxide in these structures. However, recently, in the structures oxide/SiC(Si), oxides of titanium [1–5] and rare earth elements (REE) [7–10], the so-called alternative dielectrics (dielectrics with high permittivity – high-*k* dielectrics), are considered as oxides [11–15]. In addition to a high value of dielectric permittivity and band gap width, these oxides have high transparency in the visible spectral range, chemical and thermal stability [20, 21].

The optical, mechanical, and electrical characteristics of the oxide film/SiC structure are affected by both the microscopic nature of the surface relief and the mechanical stresses arising in the structure. The inhomogeneous spatial distribution of interfacial states at the oxide film/SiC interface, due to different local electronic structures for different SiC crystallographic directions, or with different configurational environments of impurity atoms (often nitrogen), can cause a non-uniform distribution of electrical properties caused by spatial fluctuations of the surface potential [6]. For example, in the work [22] it was shown that in SiO_2 films on a silicon carbide substrate owing to different values of internal mechanical stresses at the SiO_2/SiC interface for the films grown by various methods, a shift in the

© V. Lashkaryov Institute of Semiconductor Physics of the NAS of Ukraine, 2023
© Publisher PH "Akademperiodyka" of the NAS of Ukraine, 2023

maximum of the PL spectrum is observed. A slight change in the position of PL band maximum for the samples with different ways for creation of the thin SiO_2 film is a consequence of the redistribution of defects localized at the SiO_2/SiC interface with a change in the internal mechanical strains value at the SiO_2/SiC interface [22].

The main reasons for the occurrence of internal strains in the oxide film/substrate structures are as follows: 1) the difference in the coefficients of thermal expansion of the film and substrate, leading to the appearance of thermal stresses; 2) mismatch between the crystal lattices of the film and substrate, resulting in mismatch strains; 3) the presence of internal strains due to phase inhomogeneities and structural defects in the material of the film and substrate.

The oxidation process involves several physical phenomena, including the diffusion of oxygen atoms into the metal film, the reaction of oxygen with metal atoms to form metal oxide, and the migration of metal and oxide ions. The rate of these processes can be influenced by such factors as annealing temperature and time, oxygen pressure, and the properties of the original metal film. For instance, a higher annealing temperature can increase the diffusion rate and reaction rate, leading to more complete oxidation. However, it could also introduce more defects due to the increased mobility of atoms. The volume change associated with the oxidation reaction is another stress source, inducing compressive stress in the film. The magnitude of these stresses can influence the density and type of defects in the film, namely: dislocations, vacancies and grain boundaries, which can, in turn, affect the film electrical and optical properties.

Since REE oxides are usually synthesized at lower temperatures than SiO_2 oxide, it can be expected that the films based on REE oxides will not cause significant mechanical stresses at the REE oxide/semiconductor substrate interface. At the same time, for oxides of titanium and rare-earth elements, the impact of mismatched stresses on the properties of the OP structure, where silicon carbide acts as a semiconductor, will be much higher than that for the SiO_2/SiC structure. There is still a lack of published information regarding the local homogeneity of these REE oxide films and how it affects the physical properties of thin-film structures.

The aim of this work is to evaluate internal mechanical stresses and to analyze their influence on nanomorphology and local resistive properties of the surface, as well as their relationship with the optical characteristics of TiO_2(Gd_2O_3, Er_2O_3)/SiC thin oxide film structures in comparison with SiO_2/SiC structures.

2. Samples and research methods

Metal oxide films were synthesized using the rapid thermal annealing (RTA) of titanium, erbium, and gadolinium metal films deposited on SiC substrates *via* thermal sputtering. The RTA oxidation was performed at 350 °C in oxygen atmosphere.

The surface nanomorphology and the corresponding local distributions of the film specific resistivity were studied using scanning spreading resistance microscopy (SSRM) with a NanoScope IIIa Dimension 3000TM scanning probe microscope [6, 23–25]. Platinum probes with a nominal tip radius of 20 nm were used. The bias voltage did not exceed 5 V. The optical properties of the structures were characterized on the basis of the transmission and photoluminescence (PL) spectra. Absorption and PL spectra were recorded using the SDL-2 setup within the range $\lambda = 400\ldots800$ nm. A SIRSh-200 spectral lamp was used as a continuous spectrum source for measuring the transmission spectra. Nitrogen laser radiation ($\lambda_{ex} = 337$ nm) was used to excite the PL spectra. All the optical measurements were carried out at room temperature.

3. Comparative evaluation of mechanical stresses in oxide film/SiC structures

To estimate the total mechanical stress, we systematically analyzed each of the strain components and their relative magnitude by using the common models of thin film mechanics. The stresses can be additive or partially relaxed due to plastic deformation. The total stress σ in a thin film that is formed on a thick substrate is expressed using the formula $\sigma = E_f\,\varepsilon_{tot}$, where E_f is the film elastic modulus and ε_{tot} is the total strain. The total strain has components $\varepsilon_{tot} = \varepsilon_{th} + \varepsilon_{lm} + \varepsilon_{ox} + \varepsilon_{gb}$, where ε_{th}, ε_{lm}, ε_{ox}, ε_{gb} are the thermal mismatch, lattice mismatch, oxidation and grain boundary stresses, respectively. The oxidation and grain boundary stresses represent the internal strains due to the phase inhomogeneities and structural defects [26, 27].

The most common consideration for thin film structures is biaxial deformation. The biaxial stress state implies stresses parallel ($\sigma_{||}$) and perpendicular ($\sigma_{\perp}$) to the film plane. In our estimations, we assume coherent stresses ($\sigma_{||} = \sigma_{\perp}$), $\sigma_{||} = E_f/(1-\nu)\varepsilon_{tot}$ where ν is the Poisson ratio for the film. However, it should be noted that if the film relaxes, the strain may become non-equi-biaxial.

The thermal strain between the film and substrate is $\varepsilon_{th} = (\alpha_f - \alpha_s)\Delta T$, where α_f, α_s refer to the thermal expansion coefficients of the film and substrate, respectively [28]. ΔT is the difference in temperature between the stress-free deposition temperature and the observation temperature. The intrinsic misfit strain between the film and substrate due to lattice parameter mismatch is $\varepsilon_{lm} = (a_f - a_s)/a_s$, where a_f, a_s are the lattice parameters [28]. In the course of oxidation process, the molar volume increases due to incorporation of oxygen according to the expression $\Delta V/V = (M_f - M_i)/(\rho M_i)$, where M_f and M_i are the molar masses per unit volume before and after oxidation, and ρ is the density of the oxidized film. It is the origin of oxidation strain ε_{ox}. Finally, for a nanocrystalline film,

Table 1. Data used for the estimates of mechanical stresses in $TiO_2(Gd_2O_3, Er_2O_3, SiO_2)/SiC$ structures. Lattice parameters (a, c), thermal expansion coefficient ($\alpha_{f,s}$), Poisson's ratio (ν_f), elastic modulus ($E_{f,s}$), film thickness ($d_{f,s}$) and β – grain boundary free energy per unit area.

	a, nm	c, nm	$\alpha_{f,s}\times10^6$ °C^{-1}	ν_f	$E_{f,s}$, GPa	β, J/m^2	$d_{f,s}$, nm
SiC	0.309	1.05(4*H*) 1.51(6*H*)	~3 [29]	0.16	392	1.5	~500·10^3
TiO_2	0.459[30]	0.295 [30]	8.3 [30]	0.32 [30]	244 [30]	0.60	~65 [32]
Gd_2O_3	0.376[30]	0.589 [30]	10 [30]	0.26 [30]	150 [30]	0.75	~70 [32]
Er_2O_3	1.005[30]		10.5 [30]	0.338 [31]	177 [31]	0.87	~150 [32]
SiO_2	0.491	0.540	~0.5 [30]	0.17 [30]	71 [30]	0.35	~70 nm [22]

Table 2. Estimates of mechanical stresses in $TiO_2(Gd_2O_3, Er_2O_3)/SiC$ structures: thermal (σ_{th}), lattice mismatch (σ_{lm}), oxidation stress (σ_{ox}) and grain boundary stress (σ_{gb}). Typical stress values for similar structures as observed experimentally (σ).

	σ_{th}, GPa	σ_{lm}, GPa	σ_{ox}, GPa	σ_{gb}, GPa	σ, GPa
TiO_2	0.62	0.523	61	0.003	0.65 tensile [33–35]
Gd_2O_3	0.46	0.13	36	0.003	0.60 tensile [36, 37]
Er_2O_3	0.65	1.8	39	0.003	0.70 tensile [38]
SiO_2	–0.24	0.15	37	0.007	0.30 tensile [34, 35, 39]

additional strain can develop due to grain boundary formation. The common model for grain boundary strain is $\varepsilon_{gb} = \beta/(E_f D)$, where β is the grain boundary free energy per unit area, D is the grain size, and ε_{gb} represents the dilatational misfit.

Since the investigated films contain amorphous phase and are polycrystalline rather than single crystal oriented, we cannot simply use the lattice mismatch formula for ε_{lm}, assuming direct epitaxial lattice matching. Inaccuracies in analyzing the lattice contribution to strain can be minimized by considering various factors, such as the distribution of grain orientations in the film relatively to the SiC substrate, the impact of lattice rotation and alignment between grains in the film and SiC surface, as well as the average coherent lattice matching strain over different orientations. Assuming hexagonal closed packed structure, there are mainly two types of grain orientations – basal plane parallel to substrate (c-axis normal) and prismatic plane parallel (c-axis in plane). The basal orientation exhibits lower lattice mismatch strain because of the better fit between closely-packed planes. The prismatic orientation results in greater mismatch, caused by the alignment of open lattice planes with the substrate. The effective averaged lattice mismatch strain was estimated using the predominance of basally oriented grains.

Simple volume conservation arguments of the Pilling–Bedworth type are obviously insufficient in themselves, but experimental trends suggest that some volume conservation principle may be involved as a starting point [28]. Estimating grain boundary energies for oxides without specific experimental data is also challenging. In materials science, it is a widely accepted principle that the grain boundary energy is related to the surface energy of the material. It has been observed that in many materials, the grain boundary energy is roughly 50% of the surface energy. These values were used in our estimations.

The data used for estimating the results of the above-described evaluations are summarized in Tables 1 and 2.

The obtained results of estimating the stresses in $SiO_2(TiO_2, Gd_2O_3, Er_2O_3)/SiC$ structures showed that in all cases these strains are tensile; moreover, the minimum strain values can be expected in SiO_2 and Gd_2O_3 films. The maximum strain value is predicted for Er_2O_3 films (see Table 2). It should be noted that the granular structure of the films (grain boundaries) will make a minimal contribution to the integral strains of the structure. In this case, the ratio of the nanocrystalline and amorphous phases in films should be taken into account, which, in turn, will also affect the level of misfit strains.

It is assumed that the thermal strains in the films of Ti, Er, and Gd metals deposited on a silicon carbide substrate to form an oxide layer by treatment in oxygen will be approximately equal. In this case, silicon oxide films are special due to the opposite sign of thermal strain. As for the Er_2O_3 films, when texturing the granular structure of these films, one should expect a significant increase in misfit strains. The level of these strains can be an order of magnitude higher than those in Gd_2O_3 films. For TiO_2 films, one should expect an increased susceptibility to the quality of oxidation, since the increase in bulk strain of the oxide phase is almost two times higher than the values for other films under consideration. It is important to note that the provided values were used for a rough comparison of the factors that influence the level of mechanical stress in thin films, and this was done using the very basic models for estimation purposes. The actual stress values in films are influenced by a multitude of factors including the specifics of films formation, their structural characteristics and the relaxation processes involved. Stress values reported in the literature for analogous structures exhibit substantial variation, with reported values spanning from several hundred megapascals to a few gigapascals.

4. Experimental results and discussion

As shown in [32], in all cases the surface of Er, Ti, Gd oxide films on a silicon carbide substrate is inhomogeneous in phase composition and has an island character. As the oxidation time increases, the island density increases. In this case, the TiO_2 oxide film retains a granular texture, while the Gd_2O_3 and Er_2O_3 films start to exhibit surface grain aggregation as oxidation time progresses. One result of this granular surface in oxide films is a nonuniform distribution of conductivity across the films, among other effects.

Fig. 1 presents the data obtained from scanning spreading resistance microscopy (SSRM) for TiO_2/SiC and Er_2O_3/SiC structures. Additionally, Fig. 1 includes SSRM data for SiO_2/SiC structures, which were obtained through thermal oxidation at a temperature of 1150 °C, for comparison.

One advantage of the SSRM method is its ability to monitor physicochemical processes in surface layers by identifying changes in local electrophysical properties. The high sensitivity of this technique, which measures resistances ranging from 10^2 to 10^{14} Ohm, enables the detection of alterations in the concentration and mobility of charge carriers in surface layers. These alterations are associated, in part, with the influence of mechanical stresses on defect formation processes on the oxide surface. The resistivity of the films, as determined by SSRM, offers insight into the electrical properties of the film associated with carrier mobility and concentration, and can be related to these physical processes and the structural integrity of the films.

The Er_2O_3 film displays a nanocrystalline grain structure (Fig. 1a), but with a more uniform grain size distribution around 200…300 nm (Figs 1a, 1g, curve *a*). This is evident in the relatively smooth granular morphology of the surface. The larger 34 nm surface roughness arises from sporadic growth of large 1500 nm diameter hillocks on the surface. These are seeded by defects that initiate uncontrolled precipitation, reflecting spatial inhomogeneity in structural perfection. Concerning to TiO_2, the submicron-scale regions of lower resistivity result from interrelated transport along grain boundaries and oxygen vacancies. The polycrystalline structure with random grain orientations creates discontinuities along the grain boundaries, which concentrates current. The large hillocks likely act as localized current leakage channels due to high defect densities. This enables resistivity reduction to extend over longer scales as compared to the other films. In addition, the annealing temperature close to 350 °C may result in incomplete oxidation of the full 150 nm Er layer. Metallic Er has much higher conductivity than Er_2O_3, so any unoxidized metallic Er regions along grain boundaries would further reduce local resistivity. Overall, the polycrystalline structure and high surface roughness creates low resistivity paths on the scale of 1 to 5 µm vertically in the Er_2O_3 film. As can be seen from the SSRM data, Er_2O_3 films are characterized by the maximum value surface-averaged local resistivity – 50 MOhm·cm (Figs 1b, 1h, curve *a*).

The TiO_2 film likely has a nanocrystalline structure, leading to more pronounced variation in the local resistivity (Figs 1c, 1g, curve *c*). The TiO_2 film has a sufficiently higher roughness of 11 nm, indicating a textured surface and relatively larger grains (150…300 nm). This higher roughness suggests that the film has a higher density of surface defects, which can be attributed to the high mechanical stresses and low homogeneity of TiO_2 film.

The three-fold higher thermal expansion coefficient of TiO_2 as compared to that of SiC produces a compressive stress around 0.6 GPa during cooling. This high stress can cause incomplete oxidation and residual metallic Ti grains or regions along grain boundaries. Metallic Ti has resistivity orders of magnitude lower than TiO_2. Overall, the nanocrystalline structure and high compressive stress in TiO_2 leads to local resistivity variations on the scale of the grain size, around 50…300 nm (Figs 1c, 1g, curve *c*). The overall resistivity of the TiO_2 film is 10 MOhm·cm, which significantly less than the resistivity of the Er_2O_3 films (Figs 1d, 1h, curves *a*, *b*).

The SiO_2 film has the lowest roughness of 3 nm, which indicates a relatively smooth surface (Figs 1e, 1g, curve *e*). This low roughness suggests that the film has a low density of surface defects such as hillocks and voids, which can be attributed to the low thermal expansion mismatch between SiO_2 and SiC as well as the low intrinsic strain in the SiO_2 film. The SiO_2 film on SiC is

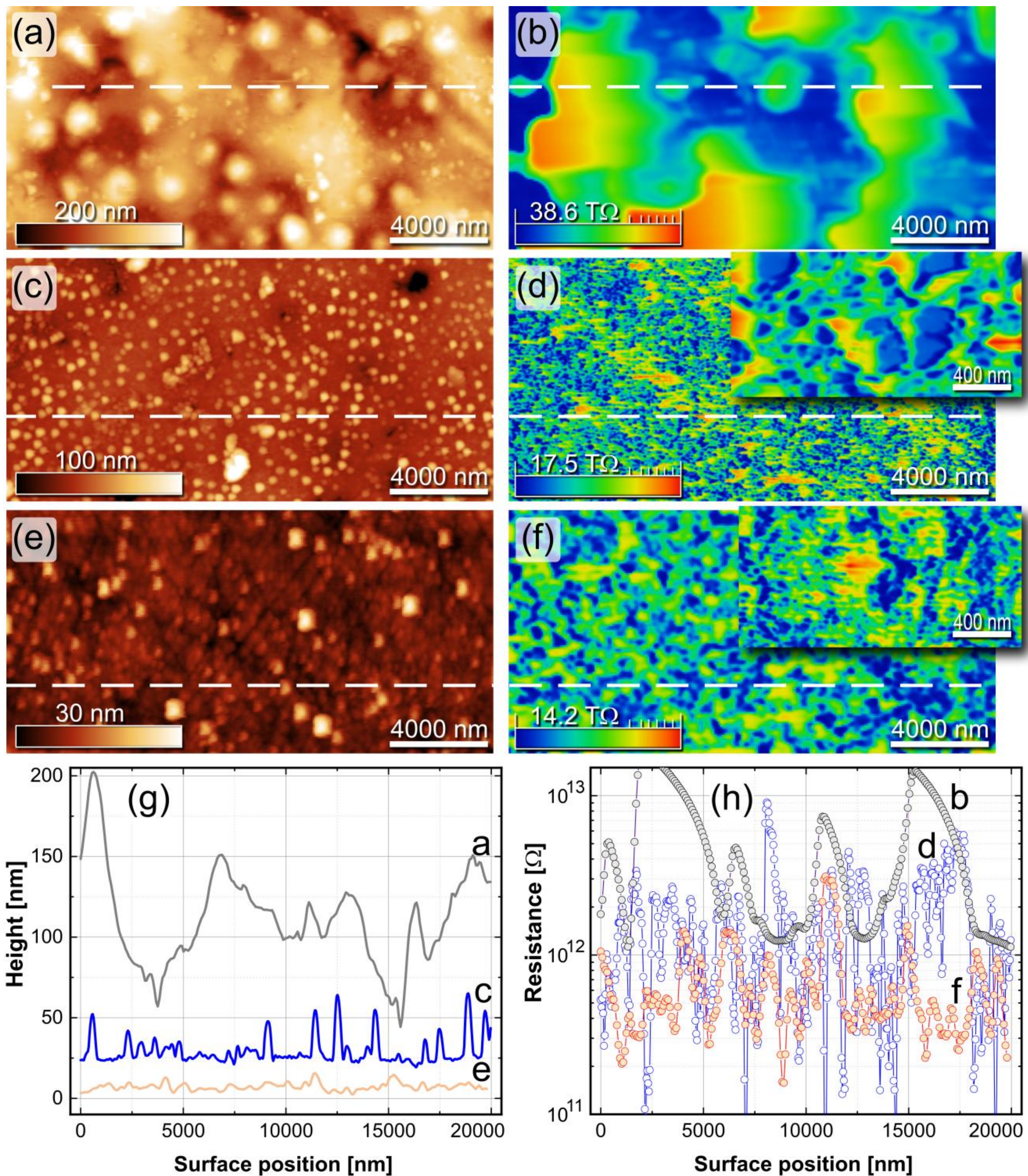

Fig. 1. Related SSRM height and resistance maps for Er_2O_3 (a, b), TiO_2 (c, d) and SiO_2 (e, f) films. Corresponding cross-sections of the maps along the dashed lines are shown in (g, h).

expected to be amorphous and have the relatively uniform resistivity, with only small localized regions of lower resistivity. This is because SiO_2 readily forms a stable amorphous oxide during thermal deposition. The amorphous structure lacks grain boundaries or defects that could lead to localized current pathways.

The resistivity of SiO_2 film is 6 MOhm·cm, which is less than that of titanium oxide films and significantly less than that of erbium oxide films (Fig. 1h). It suggests that the film has a low density of defects, namely: vacancies and dislocations. However, the thermal oxidation process can result in some non-uniformity and

non-stoichiometric SiO_x regions, if oxidation is incomplete. Any residual unoxidized Si or SiO_x will have higher conductivity than SiO_2. But since oxidation rates of SiC are relatively rapid, these regions are expected to be small, less than 60 nm in size. This reflects the local resistance SSRM map and the corresponding cross-section (Figs 1f, 1h, curve *f*).

As can be seen from Fig. 1, the surface morphology of the thin films, as reflected in their roughness and grain size, is closely related to the local resistivity of the films, *i.e.* homogeneity (Fig. 1). The roughness and grain size can be influenced by the stress in the film and the physical processes during oxidation. For instance, high stress can lead to a rougher surface and larger grains, as the film seeks to minimize the stress by forming a more relaxed grain structure. This can increase the resistivity, since grain boundaries can act as barriers to electron transport, thereby increasing the scattering of electrons and hence the resistivity.

On the other hand, a smoother surface and smaller grains, as in the case of the SiO_2 film, can lead to lower resistivity. The smoother surface reduces the scattering of electrons at the surface, while the smaller grains increase the density of grain boundaries, which can act as pathways for electron transport, thereby reducing the resistivity.

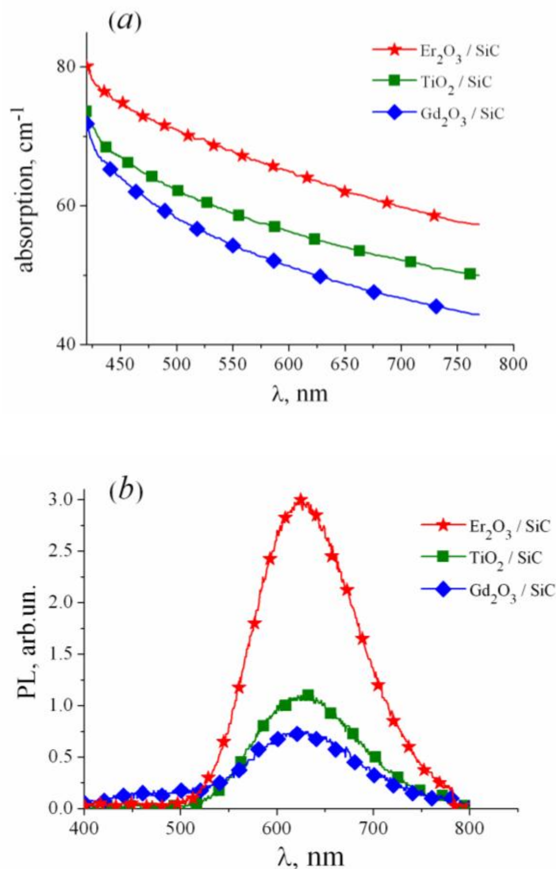

Fig. 2. Absorption spectra in the transparency range of the SiC substrate ($E_{g\,\mathrm{SiC}}$ = 3.2 eV) (a), and PL spectra (λ_{exc} = 337 nm, $h\nu_{exc} \approx 3.68$ eV) (b) of $TiO_2(Gd_2O_3, Er_2O_3)$/SiC structures. The PL spectrum of the SiC substrate without an oxide film was used as a reference to compare the PL spectra.

Fig. 2a shows the absorption spectra of $TiO_2(Gd_2O_3, Er_2O_3)$ structures in the transparency region of the SiC substrate ($E_{g\,\mathrm{SiC}}$ = 3.2 eV). When analyzing the transmission and photoluminescence spectra of the analyzed structures, it should be taken into account that these spectra are an integral characteristic of the structure, as in the case of SiO_2/SiC structures [22]. Therefore, in the absorption spectra of samples, their absorption edge is defined by the structure component that has the smallest band gap. In this case, such a structural element is a silicon carbide substrate (see Table 1). The relatively low concentrations of impurity atoms both in the oxide film and in the substrate (in particular, impurities of boron and nitrogen typical for silicon carbide [40]) are evidenced by the absence of individual absorption bands in the transmission spectrum of the oxide film/silicon carbide structures (Fig. 2a).

The characteristic features of the luminescence spectra of the oxide film/substrate structure (Fig. 2b) are also determined by several factors: the PL spectrum of the metal oxide film itself, the degree of transparency of the metal oxide film both in the excitation radiation region and in the silicon carbide luminescence region, and is an integral PL spectrum of proper film and silicon carbide.

Fig. 2b shows the photoluminescence spectra of the $TiO_2(Gd_2O_3,Er_2O_3)$/SiC heterostructures (PL was excited from the side of the oxide film). A comparative analysis of the PL spectra measured from the side of the metal oxide film and from the side of silicon carbide showed that the spectral composition of the PL band of the metal oxide film/silicon carbide structure is mainly caused by the contribution of silicon carbide. The absence of bands characteristic of the PL of REE oxides in the PL spectra can be explained by the fact that the PL intensity of silicon carbide significantly exceeds the PL intensity of thin films of REE oxides.

The observed SiC PL band with a maximum at 630 nm is associated in the literature [40–42] with radiative transitions in the centers impurity (nitrogen) – defect or impurity – vacancy (usually, the carbon vacancy is considered). In the earlier work [43], this band was associated with recombination processes caused by the presence of defects near the surface of a silicon carbide crystal.

As can be seen from Fig. 2, there is a correlation between the absorption and PL spectra of the $TiO_2(Gd_2O_3, Er_2O_3)$/SiC structures: with an increase in the absorption coefficient, the PL intensity increases.

It should be noted that TiO_2 Gd_2O_3 and Er_2O_3 oxide films were obtained at the same temperature. At the same time, a change in the method of forming the thin SiO_2 film on the surface of silicon carbide, which was accompanied, among other things, by a change in the

temperature of obtaining the oxide, led to a change in the position of the maximum of the PL band for samples with different methods of forming a thin film [22]. In this case, the optical absorption spectra of the SiO_2/SiC structures almost coincided [22].

Structural disordering caused by the mismatch of crystal lattices in the PL spectra is reflected by the change in PL characteristics of the upper silicon carbide layer adjacent to the oxide film/SiC interface. The energy position and normalized shape of the PL lines completely coincide for the structures TiO_2(Gd_2O_3, Er_2O_3)/SiC. At the same time, the PL intensity in the Gd_2O_3/SiC structures is almost 1.5 times lower than in the TiO_2/SiC structures and 4 times lower than in the Er_2O_3/SiC structures. It means that at room temperature, in the Er_2O_3/SiC and TiO_2/SiC structures, in contrast to the Gd_2O_3/SiC structures, there is a significant concentration of radiative recombination centers.

As can be seen from Fig. 2, the observed changes in the PL intensity and in the absorption coefficient of the TiO_2 (Gd_2O_3, Er_2O_3)/SiC structures correlate with the value of σ_f – misfit strain (see Table 2). Thus, the maximum PL intensity (~3 arb. units) and the maximum values of the absorption coefficient (~63 cm^{-1} for λ = 630 nm) are observed for the Er_2O_3/SiC structures, for which the value of misfit stresses is maximum (see Table 2). In this case, additional defects, which are PL centers, may appear at the Er_2O_3/SiC interface. At the same time, the Gd_2O_3/SiC interface is characterized by a minimum amount of defects caused by misfit stresses in the oxide film/substrate structures (see Table 2). In this case, the PL intensity at the maximum of the band for the Gd_2O_3/SiC structures is ~0.73 arb. un., and the value of the absorption coefficient for λ = 630 nm is ~50 cm^{-1}. For TiO_2/SiC structures, an intermediate situation is observed: at misfit stresses (see Table 2), the PL intensity at the band maximum for TiO_2/SiC structures is ~1.1 arb. un., and the value of the absorption coefficient for λ = 630 nm is ~55 cm^{-1}.

5. Conclusions

This study elucidated the interrelations between internal mechanical strains, surface morphology, nano-scale electrical properties, and optical characteristics in TiO_2, Gd_2O_3, Er_2O_3, and SiO_2 thin films on SiC substrates. The oxide films were synthesized *via* rapid thermal annealing and analyzed using scanning spreading resistance microscopy, photoluminescence and absorption spectroscopy. Estimations of strain components revealed net tensile stresses arising from thermal mismatch, lattice mismatch, oxidation, and grain boundaries. Scanning spreading resistance microscopy demonstrated that surface roughness and grain structure correlated with spatial variations in resistivity, attributed to conductive pathways along boundaries and possible metallic phases. Photoluminescence intensity has also been found to correlate with estimated lattice mismatch strain.

Gd_2O_3/SiC has exhibited the least amount of defects, while Er_2O_3 and TiO_2 have shown a higher amount, with Er_2O_3 being most mismatched and roughest. The appearance of PL centers of a different nature, as was observed in the SiO_2/SiC structures [22], was not seen in the TiO_2 (Gd_2O_3, Er_2O_3)/SiC structures. These results demonstrate that internal strains in oxide thin films on SiC substrates can influence surface morphology, leading to formation of defects and spatial inhomogeneity. The associated fluctuations in local conductivity and density of luminescence centers have important implications for both dielectric and optical applications.

Overall, this work reveals the multiscale connections between film stresses, nanoscale electrical and optical properties, as well as ultimate thin film performance. These insights pave the way for future processing refinements to mitigate internal strains in order to improve the functionality of oxide thin films for both semiconductor and optical technologies.

References

1. Gyanan, Mondal S., Kumar A. Tunable dielectric properties of TiO_2 thin film based MOS systems for application in microelectronics. *Superlattices Microstruct*. 2016. **100**. P. 876–885 https://doi.org/10.1016/j.spmi.2016.10.054.
2. Chiappim W., Watanabe M., Dias V., Testoni G. *et al.* MOS capacitance measurements for PEALD TiO_2 dielectric films grown under different conditions and the impact of Al_2O_3 partial-monolayer insertion. *Nanomaterials.* 2020. **10**. P. 338. https://doi.org/10.3390/nano10020338.
3. Cetin S.S., Efkere H.I., Sertel T. *et al.* Electrical properties of MOS capacitor with TiO_2/SiO_2 dielectric layer. *Silicon*. 2020. **12**. P. 2879–2883. https://doi.org/10.1007/s12633-020-00383-8.
4. Roy S.K., Ibanez J.U., O'Neill A. *et al.* Characterisation of 4H-SiC MOS capacitor with a protective coating for harsh environments applications. *Mater. Sci. Forum*. 2017. **897**. P. 327–330. http://dx.doi.org/10.4028/www.scientific.net/msf.897.327.
5. Saari J., Ali-Löytty H., Honkanen M. *et al.* Interface engineering of TiO_2 photoelectrode coatings grown by atomic layer deposition on silicon. *ACS Omega*. 2021. **6**, No 41. P. 27501–27509. https://doi.org/10.1021/acsomega.1c04478.
6. Fiorenza P., Giannazzo F., Roccaforte F. Characterization of SiO_2/4H-SiC interfaces in 4H-SiC MOSFETs: A review. *Energies*. 2019. **12**, No 12. P. 2310. https://doi.org/10.3390/en12122310.
7. Kahraman A., Deevi S.C., Yilmaz E. Influence of frequency and gamma irradiation on the electrical characteristics of Er_2O_3, Gd_2O_3, Yb_2O_3, and HfO_2 MOS-based devices. *J. Mater. Sci*. 2020. **55**. P. 7999–8040. https://doi.org/10.1007/s10853-020-04531-8.

8. Kahraman A. Understanding of post deposition annealing and substrate temperature effects on structural and electrical properties of Gd_2O_3 MOS capacitor. *J. Mater. Sci: Mater. Electron*. 2018. **29**. P. 7993–8001. https://doi.org/10.1007/s10854-018-8804-y.
9. Wu Q., Yu Q., He G. *et al*. Interface optimization and performance enhancement of Er_2O_3-based MOS devices by ALD-derived Al_2O_3 passivation layers and annealing treatment. *Nanomaterials.* 2023. **13**. P. 1740. https://doi.org/10.3390/nano13111740.
10. Morkoc B., Kahraman A., Aktag A., Yilmaz E. Electrical parameters of the erbium oxide MOS capacitor for different frequencies. *Celal Bayar University Journal of Science.* 2019. **15**, No 2. P. 139–143. https://doi.org/10.18466/cbayarfbe.460022.
11. Wang B., Huang W., Chi L. *et al.* High-*k* gate dielectrics for emerging flexible and stretchable electronics. *Chem. Rev*. 2018. **118**. No 11. P. 5690–5754. https://doi.org/10.1021/acs.chemrev.8b00045.
12. Liu L.N., Tang W.M., Lai P.T. Advances in La-based high-k dielectrics for MOS applications. *Coatings.* 2019. **9**, No 4. P. 217. https://doi.org/10.3390/coatings9040217.
13. Radamson H.H., Luo J., Simoen E., Zhao C. *CMOS Past, Present and Future*. Woodhead Publ., 2018. https://doi.org/10.1016/C2016-0-03462-9.
14. Das S. (Ed.) *2D Materials for Electronics, Sensors and Devices Synthesis, Characterization, Fabrication and Application.* Elsevier, 2023. https://doi.org/10.1016/C2019-0-00305-6.
15. Dimitrakis P., Valov I., Tappertzhofen S. (Eds.) *Metal Oxides for Non-volatile Memory: Materials, Technology and Applications.* Elsevier, 2022. https://doi.org/10.1016/C2017-0-01762-7.
16. Alshammari A.H., Alshammari M., Ibrahim M. *et al.* New hybrid PVC/PVP polymer blend modified with Er_2O_3 nanoparticles for opto-electronic applications. *Polymers*. 2023. **15**. P. 684. https://doi.org/10.3390/polym15030684.
17. Yang H., Yang B., Chen W., Yang J. Preparation and photocatalytic activities of TiO_2-based composite catalysts. *Catalysts*. 2022. **12**. P. 1263. https://doi.org/10.3390/catal12101263.
18. Mohamed H.E.A., Khalil A.T., Hkiri K. *et al.* Physicochemical and nanomedicine applications of phyto-reduced erbium oxide (Er_2O_3) nanoparticles. *AMB Exp.* 2023. **13**. Art. No 24. https://doi.org/10.1186/s13568-023-01527-w.
19. Chai H., Zheng Z., Liu K. *et al*. Stability of metal oxide semiconductor gas sensors: A review. *IEEE Sens. J*. 2022. **22**. P. 5470–5481. https://doi.org/10.1109/JSEN.2022.3148264.
20. Pustovarov V.A., Nikolaev R.E., Trifonov V.A. *et al*. Gadolinium oxide single crystals: Optical properties and radiation resistance. *Opt. Mat*. 2023. **141**. P. 113966. https://doi.org/10.1016/j.optmat.2023.113966.
21. Soussi A., Hssi A.A., Boujnah M. *et al.* Electronic and optical properties of TiO_2 thin films: Combined experimental and theoretical study. *J. Electron. Mater.* 2021. **50**. P. 4497–4510. https://doi.org/10.1007/s11664-021-08976-8.
22. Bacherikov Yu.Yu., Boltovets N.S., Konakova R.V. *et al.* Interface features of SiO_2/SiC heterostructures according to methods for producing the SiO_2 thin films. *Semiconductor Physics, Quantum Electronics & Optoelectronics.* 2012. **15**, No 1. P. 13–16. https://doi.org/10.15407/spqeo15.01.13.
23. De Wolf P., Snauwaert J., Clarysse T. *et al*. Characterization of a point-contact on silicon using force microscopy supported-resistance measurements. *Appl. Phys. Lett*. 1995. **66**. P. 1530–1532. https://doi.org/10.1063/1.113636.
24. Swanson L.K., Fiorenza P., Giannazzo F. *et al*. Correlating macroscopic and nanoscale electrical modifications of SiO_2/4H-SiC interfaces upon post-oxidation-annealing in N_2O and $POCl_3$. *Appl. Phys. Lett.* 2012. **101**. P. 193501. https://doi.org/10.1063/1.4766175.
25. Ulyashin A., Sytchkova A. Hydrogen related phenomena at the ITO/a-Si:H/Si heterojunction solar cell interfaces. *phys. status solidi (a).* 2013. **210**, No 4. P. 711–716. https://doi.org/10.1002/pssa.201200459.
26. Abadias G., Chason E., Keckes J. *et al*. Review Article: Stress in thin films and coatings: Current status, challenges, and prospects. *J. Vac. Sci. Technol. A*. 2018. **36**. P. 020801. https://doi.org/10.1116/1.5011790.
27. Zhou X., Yu X., Jacobson D, Thompson G.B. A molecular dynamics study on stress generation during thin film growth. *Appl. Surf. Sci*. 2019. **469**. P. 537–552. https://doi.org/10.1016/S0010-938X(70)80036-1.
28. Stringer J. Stress generation and relief in growing oxide films. *Corrosion Science*. 1970. **10**. P. 513–543. https://doi.org/10.1016/S0010-938X(70)80036-1.
29. Stockmeier M., Sakwe S.A., Hens P. *et al*. Thermal expansion coefficients of 6H silicon carbide. *Mater. Sci. Forum*. 2008. **600–603**. P. 517–520. https://doi.org/10.4028/www.scientific.net/msf.600-603.517.
30. Samsonov G.V. Thermal and Thermodynamic Properties. In: Samsonov, G.V. (ed.) *The Oxide Handbook*. Boston, MA, Springer, 1973. https://doi.org/10.1007/978-1-4615-9597-7_3.
31. Rittenhouse T.L., Bohn P.W., Hossain T.K. *et al.* Surface-state origin for the blueshifted emission in

anodically etched porous silicon carbide. *J. Appl. Phys*. 2004. **95**. P. 490–496. https://doi.org/10.1063/1.1634369.

32. Bacherikov Y.Y., Dmitruk N.L., Konakova R.V. *et al.* Effect of rapid thermal annealing on the properties of thin dielectric films of gadolinium, titanium, and erbium oxides on the silicon carbide surface. *Tech. Phys.* 2007. **52**. P. 253–257. https://doi.org/10.1134/S106378420702017X.
33. Matěj Z., Kužel R., Nichtová L. XRD total pattern fitting applied to study of microstructure of TiO_2 films. *Powder Diffraction*. 2010. **25**, No 02. P. 125–131. https://doi.org/10.1154/1.3392371.
34. Sankur H., Gunning W. Sorbed water and intrinsic stress in composite TiO_2-SiO_2 films. *J. Appl. Phys.* 1989. **66**. P. 807–812. https://doi.org/10.1063/1.343501.
35. Vretenar P. The stress reduction in TiO_2 films. *Vacuum*. 1990. **40**. P. 173–175. https://doi.org/10.1016/0042-207X(90)90148-R.
36. Xiang W.F., Ni H., Lu H.B. In situ RHEED analysis of epitaxial Gd_2O_3 thin films grown on Si (001). *Appl. Phys. A*. 2013. **110**. P. 423–426. https://doi.org/10.1007/s00339-012-7231-9.
37. Ulloa-Castillo N.A., Lastras-Martínez L.F., Balderas-Navarro R.E. *et al.* Measurement of the shear strain of the Gd_2O_3/GaAs(001) interface by photoreflectance difference spectroscopy. *Appl. Phys. Lett*. 2014. **105**. P. 181905. https://doi.org/10.1063/1.4901168.
38. Liu Z., Yu G., He A., Wang L. Simulation of thermal stress in Er_2O_3 and Al_2O_3 tritium penetration barriers by finite-element analysis. *Plasma Sci. Technol.* 2017. **19**. P. 095602. https://doi.org/10.1088/2058-6272/aa719d.
39. Liu L., Tang W., Zheng B.-X., Zhang H.-X. Fabrication and characterization of SiC thin films. *2011 6th IEEE Int. Conf. on Nano/Micro Engineered and Molecular Systems*, Kaohsiung, Taiwan, 2011. P. 146–149. https://doi.org/10.1109/NEMS.2011.6017316.
40. Gorban' I.S., Krokhmal' A.P. The impurity optical absorption and conduction band structure in 6*H*-SiC. *Semiconductors.* 2001. **35**. P. 1242–1248. https://doi.org/10.1134/1.1418064.
41. Patrick Lyle, Choyke W.J. Photoluminescence of radiation defects in ion-implanted 6H-SiC. *Phys. Rev. B*. 1972. **5**, No 8. P. 3253–3259. https://doi.org/10.1103/PhysRevB.5.3253.
42. Choyke W.J., Patrick Lyle. Photoluminescence of radiation defects in cubic SiC: Localized modes and Jahn-Teller effect. *Phys. Rev. B*. 1971. **4**, No 6. P. 1843–1847. https://doi.org/10.1103/PhysRevB.4.1843.
43. Gorban I.S., Rudko S.N. Optical properties of silicon carbide crystals. *Soviet Phys. – Solid State*. 1963. **5**. P. 995–998.

Authors and CV

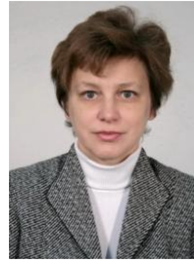

Olga B. Okhrimenko, Doctor of Science in Physics and Mathematics, Leading Researcher at the V. Lashkaryov Institute of Semiconductor Physics, NASU. Authored over 150 publications, 1 patent, 1 monograph. The area of her scientific interests includes investigation of the patterns and physical mechanisms of formation and rearrangement of the defect-impurity system of the thin-film dielectric-semiconductor structures, depending on technology of preparation, composition of thin films, additional processing and introduction of buffer layers. https://orcid.org/0000-0002-7611-4464

Yuriy Yu. Bacherikov, Doctor of Science in Physics and Mathematics, Leading Researcher at the V. Lashkaryov Institute of Semiconductor Physics, NAS of Ukraine. Authored over 300 publications, 6 patents, 1 monograph. The area of his scientific interests includes physics and applications of wide-band semiconductor compounds and devices based on them. E-mail: yuyu@isp.kiev.ua, https://orcid.org/0000-0002-9144-4592

Oksana S. Lytvyn, PhD in Physics and Mathematics, Dean of the Faculty of Information Technologies and Mathematics at Borys Grinchenko Kyiv University. Author of more than 250 publications, 2 patents, 5 chapters of textbooks. The area of her scientific interests includes theoretical modeling and digital technologies in scanning probe microscopy of physical and mechanical surface properties of various materials.
E-mail: o.lytvyn@kubg.edu.ua,
https://orcid.org/0000-0002-5118-1003

Petro M. Lytvyn, Head of Department at the V. Lashkaryov Institute of Semiconductor Physics, NASU is renowned for his expertise in semiconductor materials and systems, scanning probe microscopy, and X-ray diagnostics. Holding a PhD in Physics and Mathematics, he has authored over 350 peer-reviewed publications, significantly advancing knowledge in his fields.
E-mail: peter.lytvyn@ccu-semicond.net,
plyt@isp.kiev.ua,
https://orcid.org/0000-0002-0131-9860

Viktor Yu. Goroneskul, Researcher at the Department of Physics of Optoelectronic Devices, V. Lashkaryov Institute of Semiconductor Physics, NAS of Ukraine. Authored over 50 publications. The area of his scientific interests includes development of the sensors for monitoring environmental parameters on the basis of optron systems with open optical channel.
E-mail: goroneskul@isp.kiev.ua,
https://orcid.org/0000-0002-0697-096X

Raisa V. Konakova, Professor, Doctor of Technical Sciences, Head of the Laboratory of Physical and Technological Problems of Solid State SHF Electronics at the V. Lashkaryov Institute of Semiconductor Physics, NAS of Ukraine. The area of scientific interests of Doctor R.V. Konakova includes physics of metal-semiconductor junctions.
E-mail: konakova@isp.kiev.ua

Authors' contributions

Okhrimenko O.B.: key ideas, conceptualization, investigation, writing – original draft, supervision.
Bacherikov Yu.Yu.: key ideas, conceptualization, investigation, writing – review & editing.
Lytvyn P.M.: formal analysis, methodology, validation, data curation, writing – review and editing.
Lytvyn O.S.: formal analysis, validation, scanning probe microscopy data curation.
Goroneskul V.Yu.: investigation.
Konakova R.V.: administrator.

Взаємозв'язок між окисленням, напруженням, морфологією, локальним опором та оптичними властивостями тонких плівок TiO_2, Gd_2O_3, Er_2O_3, SiO_2 на SiC

О.Б. Охріменко, Ю.Ю. Бачеріков, П.М. Литвин, О.С. Литвин, В.Ю. Горонескуль, Р.В. Конакова

Досліджено взаємозв'язок між внутрішніми механічними напруженнями, морфологією поверхні, нанорозмірними електричними властивостями та оптичними характеристиками в тонких плівках TiO_2, Gd_2O_3, Er_2O_3 та SiO_2 на підкладках SiC. Оксидні плівки були синтезовані з використанням швидкого термічного відпалу та проаналізовані за допомогою скануючої мікроскопії опору розтікання, фотолюмінесценції та спектроскопії поглинання. У плівках були виявлені напруження, що розтягують, які пов'язані з термічною невідповідністю та невідповідністю кристалічних ґраток плівки та підкладки, окисленням і межами зерен. Ці напруження впливають на морфологію поверхні, зміни питомого опору та інтенсивності фотолюмінесценції. Було виявлено, що шорсткість поверхні та структура зерен корелюють зі змінами питомого опору, які пояснюються провідними шляхами вздовж меж зерен та можливими металевими фазами. Було також виявлено, що інтенсивність фотолюмінесценції корелює з передбачуваною деформацією невідповідності ґраток. Gd_2O_3/SiC показав найменшу кількість дефектів, у той час як Er_2O_3 і TiO_2 показали більшу кількість дефектів, причому Er_2O_3 виявився найбільш неузгодженим і найшорсткішим. Результати показують, що внутрішні напруження в тонких оксидних плівках на підкладках SiC можуть впливати на морфологію поверхні, що призводить до утворення дефектів та просторової неоднорідності. Ці флуктуації локальної провідності та щільності центрів люмінесценції мають велике значення для діелектричних та оптичних застосувань. Дослідження дає уявлення про майбутні удосконалення обробки для зниження внутрішніх напружень та підвищення продуктивності виготовлення тонких оксидних плівок у напівпровідникових та оптичних технологіях.

Ключові слова: TiO_2, Gd_2O_3, Er_2O_3, напруження, оксид/напівпровідникові структури, поглинання, фотолюмінесценція, скануюча мікроскопія опору розтікання.